Surfaceome analysis of extracellular vesicles from senescent cells uncovers uptake repressor DPP4

Qiong Meng,[a] Chen Chen,[b] Na Yang,[a] Olesia Gololobova,[c] Changyou Shi,[a] Christopher A. Dunn,[d] Martina Rossi,[a] Jennifer L. Martindale,[a] Nathan Basisty,[e] Jun Ding,[e] Michael Delannoy,[f] Srikanta Basu,[g] Krystyna Mazan-Mamczarz,[a] Chang Hoon Shin,[a] Jen-Hao Yang,[a] Peter F. Johnson,[g] Kenneth W. Witwer,[c] Arya Biragyn,[b] Payel Sen,[a] Kotb Abdelmohsen,[a] Supriyo De,[a] and Myriam Gorospe[a]

[a] Laboratory of Genetics and Genomics, [b] Laboratory of Molecular Biology and Immunology, National Institute on Aging Intramural Research Program (NIA IRP), National Institutes of Health (NIH), Baltimore, MD, USA

[c] Department of Molecular and Comparative Pathobiology, Johns Hopkins University School of Medicine, Baltimore, MD, USA

[d] Flow Cytometry Unit, [e] Translational Gerontology Branch, NIA IRP, NIH, Baltimore, MD, USA

[f] Department of Cell Biology and Imaging Facility, Johns Hopkins University School of Medicine, Baltimore, MD, USA

[g] Mouse Cancer Genetics Program, Center for Cancer Research, National Cancer Institute, Frederick, MD, USA

***Correspondence:**

Supriyo De, Myriam Gorospe, Qiong Meng

Laboratory of Genetics and Genomics

National Institute on Aging IRP

National Institutes of Health, Baltimore

251 Bayview Blvd.

Baltimore, MD 21224, USA

Email: supriyo.de@nih.gov; myriam-gorospe@nih.gov; qiong.meng@nih.gov

Supporting Information Text:

SI Appendix, Supplementary Materials and Methods

SI Appendix, Supplementary Legends to Figures and Datasets

SI Appendix, Supplementary References

Supplementary Materials and Methods

Cell culture and virus transduction. Human WI-38 diploid fibroblasts (HDFs; from Coriell Cell Repositories) human cervical carcinoma HeLa cells (from ATCC), immortalized human microglia HMC3 cells (from ATCC), and human keratinocytes HaCaT (Cell Lines Service) were cultured in Dulbecco's modified Eagle's medium (DMEM, Gibco), supplemented with 10% fetal bovine serum (FBS, Gibco), 1% antibiotics and antimycotics (Gibco), at 37°C in a humidified atmosphere of 5% CO_2; non-essential amino acids (NEAA, Gibco) were added to media; also for rat myoblast H9c2, mouse macrophages RAW 264.7 (from ATCC). Rat NR8383 macrophages (obtained from ATCC) were grown in Ham's F12K medium, supplemented with 2 mM L-glutamine 15% heat-inactivated FBS, and adjusted to contain 1.5 g/L sodium bicarbonate. The medium was also supplemented with. Human skeletal myoblasts (HSkM; from Thermo Fisher Scientific) were grown in a mixture of Ham's F10 medium and PromoCell Skeletal Muscle Cell Growth Medium, supplemented with 10% FBS. Human monocytic leukemia THP-1 cells (ATCC) were cultured in RPMI 1640 medium (Gibco) supplemented with 10% FBS, 2 mM L-glutamine, 10 mM HEPES, and 0.05 mM β-mercaptoethanol at 37°C in a humidified atmosphere of 5% CO_2. THP-1 cells were differentiated to a macrophage-like phenotype by treatment for 48 h with 150 nM phorbol 12-myristate 13-acetate (PMA). DPP4 was overexpressed in HeLa cells by infection with a lentivirus that expressed DPP4-Myc (EX-F0106-Lv125, GeneCopoeia); control viral particles expressed the Myc tag alone. The infected cells were selected by1 μg/mL puromycin treatment for 20 days to create a pool of cells used for analysis and EV collection.

Silencing and inhibition of DPP4

For silencing DPP4, pre-senescent WI-38 fibroblasts (PDL42 through PDL45) were transfected with 20 μM negative control siRNA (siCtrl, UGGUUUACAUGUCGACUAA) or DPP4 siRNAs (siDPP4, UAAGGAGGUACUCAACUUG, AUCAAAGCUAGCUACUAUA) using Lipofectamine

RNAiMAX Invitrogen) following the manufacture's protocol. Transfection efficiency was confirmed by western blot analysis.

DPP4 inhibitors used in this study include Diprotin A (Sigma-Aldrich, D3822) and Sitagliptin (Millipore Sigma, SML3205). DPP4 inhibitors were added with EVs solution and co-cultured with cells for 16 h. Doses resulting in >85% cell viability (as determined by flow cytometry analysis) were used.

Nanoparticle tracking analysis and Zeta potential measurements. The size distribution and concentration of particles were evaluated using nanoparticle tracking analysis (NTA) on a NanoSight NS300 unit with a 532-nm laser and an sCMOS camera (Malvern Panalytical), and analyzed using NanoSight NTA software v3.44. The Nanoflow cytometry analyzer (NanoFCM) was also used for measuring particle concentration and for measuring the efficiency of labeling EVs with fluorescent dyes. The NanoSight and Flow NanoAnalyzer instruments were calibrated for particle concentration and size using 250-nm Silica Beads and a Silica Nanosphere Cocktail, respectively. Following the manufacturer's instructions of Nano FCM, events were measured for one minute, and the detected events were then converted to particle size, concentration, and positive fluorescence counts. Primary antibodies recognizing DPP4 and CD81 (Invitrogen; BD Biosciences) conjugated with PE or FITC were used to validate the surface proteins of EVs. The samples were incubated for 16 h at a dilution volume of 6:1 (sample: antibody). EV Zeta Potential (1) was measured using a Zetasizer Pro (Malvern Panalytical) as follows: EVs suspended in filtered DPBS (~10^9 particles/mL) were measured using a capillary cell with a 120-s equilibration period. The 'automatic' option was selected and assessed in 10–50 runs depending on the concentration of EVs.

Western blot analysis. Proteins were extracted from total EVs using RIPA buffer (50 mM Tris-HCl (pH 7.2), 150 mM NaCl, 1% NP40, 0.1% SDS, 0.5% DOC, 1 mM PMSF, 25 mM $MgCl_2$) supplemented with HALT protease and phosphatase inhibitor cocktail (Thermo Fisher Scientific). The protein concentration was measured by Pierce BCA Protein Assay Kit (Thermo Fisher Scientific). The presence of S-EV- enriched proteins as well as EV markers was assessed in 2 μg of lysates separated on 4%-12% SDS-containing polyacrylamide gels under reducing or non-reducing conditions, respectively, and transferred onto nitrocellulose membranes (Bio-Rad Laboratories). The membranes were blocked in 5% non-fat dry milk or BSA. Primary antibodies recognizing DPP4, CD81, GAPDH, or VAT1 were used; after 1 h of incubation with appropriate secondary antibodies,

the immunoblots were developed using enhanced chemiluminescence (ECL), and the digitized images were captured using Kwik Quant Imager (Kindle Biosciences) or ChemiDoc MP (Bio-Rad Laboratories).

Transmission Electron Microscopy. Highly purified P-EVs and S-EVs were prepared for TEM as previously described. Briefly, 20 μL of EV samples (around 10^{10} particles/mL) in suspension were adsorbed to carbon-coated parlodion copper grids for 2 min, then the grids were floated on 2 consecutive drops of filtered aqueous 0.75% uranyl acetate (0.03% tylose) for 1 min each and blot dried with filter paper. Grids were viewed on a Hitachi H-7600 TEM microscope. P-EVs and S-EVs were investigated on poly-L-lysine coverslips, fixed in 1% glutaraldehyde 80 mM phosphate buffer containing 5 mM $MgCl_2$. Coverslips were rinsed in buffer with sucrose then postfixed in potassium ferrocyanide-reduced osmium tetroxide for 1 h on ice. Samples were stained en bloc in 2% uranyl acetate in maleate buffer for 1 h. After a series of progressive ethanol dehydration steps (30-100%), samples were infiltrated with Eponate 12 resin, embedded, and cured at 60°C for 48 h. After soaking in liquid nitrogen for 10 min, coverslips mounted to inverted beam capsules were carefully removed. On a Riechart Ultracut E microtome, blocks were trimmed and sectioned with a diatome diamond knife. Methanolic uranyl acetate was used to stain sections (50-60 nm), followed by incubation with lead citrate.

Specific for labeling, ultra-thin sections were picked up on formvar-coated 200-mesh nickel grids, then floated on all subsequent steps. Grids were placed on 3% sodium meta periodate for 30 min, rinsed in D-H_2O, then floated on 10 mM citrate buffer for 20 min at 95°C. Grids were then rinsed using TBS followed by a 30-min block in a TBST blocking solution containing 1% NGS and 1% BSA. DPP4 antibody (at 1:100 dilution) was incubated for 18 h at 4°C, and gold-conjugated secondary antibody (at 1:40 dilution) for 2 h. After rinsing, grids were hard-fixed in 2% glutaraldehyde in 100 mM sodium cacodylate buffer, stained with 2% uranyl acetate for 20 min, and rinsed in between with D-H_2O. Grids were viewed on a Hitachi H-7600 TEM microscope.

Mass spectrometry-based proteomics of EVs. Total and surface EV proteins were isolated from EVs obtained from WI-38 fibroblasts that were proliferating (P) (~PDL20) or rendered senescent by exposure to IR, etoposide (ETO), or exhaustion of cell division leading to replicative senescence (RS) (~PDL53). Due to challenges in obtaining adequate material for investigating the surface proteome of EVs, we included two samples from the IR and ETO groups, and performed triplicates in the P and RS groups. Mass spectrometry processing was performed by liquid chromatography-

coupled tandem MS (LS-MS/MS) using a Q-Exactive hybrid quadrupole orbitrap mass spectrometer and Nano-EasySpray Ion Source (Thermo Fisher Scientific). Raw data files acquired from each sample were searched against the human protein sequences database and UniprotKB/Swiss-Prot database using the Proteome Discoverer (v1.4) based on the SEQUEST algorithm (Thermo Fisher Scientific). The minimum peptide length specified was 5 amino acids, and the maximum false peptide discovery (FDR) rate was specified as 0.01. All assembled proteins with peptide spectrum match (PSM) counts were quantified and normalized using the normalized spectral abundance factors (NSAFs) to assign their relative abundance. The raw data, including detailed information from *SI Appendix* Datasets S7 through S17, is summarized (counts and intensity values) in *SI Appendix* Dataset S6.

We utilized the limma method in the DEP (Differential Enrichment analysis of Proteomics data) R package and used the following filters to determine which of the enriched peptides had differences that were statistically significant: fold change >1.5 and adjusted P <0.05 (2). The overlap analysis between EV proteins and human EV proteins annotated in ExoCarta were performed. To address the high rate of missing values in our dataset, we utilized data imputation to fill in the missing data and carefully assessed the impact of filtering and data imputation using the vignette at (https://bioconductor.org/packages/release/bioc/vignettes/DEP/inst/doc/MissingValues.html).

The PPI network and Gene Ontology enrichment analysis were performed in STRING (v.11.5) and Metascape (v.3.5) (3), uniport ID as input and default settings “whole genome” as statistical background. The outputs of the PPI next work were further visualized by Cytoscape (v.3.9.0) (4). GSEA was implemented with all EV surface protein sets against the reference gene sets followed by default parameters. Normalized enrichment score (NES) >1 & FDR <0.25 were selected as positively enriched genes sets. The mass spectrometry proteomics data have been deposited to MassIVE database with the dataset identifier MSV000090503 (PXD037225), and the proteomic profiles and analysis outputs included (*SI Appendix* Dataset S1-S15). EVs surface proteins was characterized with the in silico human surfaceome database (http://wlab.ethz.ch/surfaceome/) and visualized through Foamtree (https://carrotsearch.com/foamtree/) (5, 6).

Supplementary Legends to Figures and Datasets

Fig. S1. (*A*) Schematic of the EVs extraction procedure. (*B*) Representative images of S(RS)-EVs by TEM identification of embedded particles in thin sections. (*C*) Zeta potential of P-EVs and S(RS)-EVs at concentrations (10^{10} EVs/mL), measured as explained (Methods). *, $p \leq 0.05$.

Fig. S2. (*A*) Quantitative analysis of the efficiency of labeling P-EVs, S(RS)-EVs, S(IR)-EVs and S(ETO)-EVs with PKH26, as assessed by the Flow NanoAnalyzer platform. The percentages of fluorescent EVs relative to total EVs detected are indicated. (*B*) Flow cytometric analysis of the uptake of S-EVs [S(RS)-EV, S(IR)-EV, S(ETO)-EV] and P-EVs (as well as control incubations with no EVs and with PBS only) by proliferating WI-38 fibroblasts, HeLa cells, and THP-1 macrophages. ***, $p \leq 0.001$. (*C*) Representative confocal microscopy images of the uptake of P-EVs and S-EVs labeled by CFSE (as well as control incubations with no EVs and with PBS only) by P cells, HeLa cells, and THP-1 cells differentiated to macrophages.

Fig. S3. (*A*) *Left*, time-lapse video recording of RS-EVs (collected from PDL53 fibroblast) taken by THP-1 macrophages in 24 h; *right*, percentages of fluorescent cells having taken PKH26-labeled RS-EVs (*SI Appendix*, Video S1). (*B*) Time-lapsed fluorescence micrographs of PKH26-labeled S-EVs internalized in THP-1 macrophages at the times shown.

Fig. S4. (*A*) Heatmap representation of differentially abundant proteins in total EVs prepared from WI-38 P fibroblasts vs. WI-38 fibroblasts rendered senescent by RS, ETO, or IR. (*B*) Heatmap representation of six proteins differentially abundant in EVs prepared as in (*A*) depicting five proteins enriched in EVs from all three senescent groups compared with proliferating fibroblasts and one protein significantly enriched in P-EVs relative to all three senescent groups.

Fig. S5. (*A-C*). Characterization of the predicted EV surfaceome. GO enrichment analysis of the cellular components in EVs surface proteins. False discovery rate (FDR) < 0.05 was considered significant *(A)*. Comparison of 2,886 EV surfaceome proteins, (http://wlab.ethz.ch/surfaceome/ ; with 20193 proteins documented in total (June 2023), with *(B)* 73 EV surface proteins mapped on the Voronoi tree map; Log2 enrichment ratios between P-EVs and RS-EVs were mapped on the whole in silico surfaceome. The darker colors indicate higher enrichment in the surface of RS-EVs, and the

lighter colors lower enrichment. EV surface proteins are hierarchically grouped by functional classification as receptors, transporters, enzymes, miscellaneous, and unclassified. *(C) Left*, pie chart shows the percentages of EV surface proteins (456) that are documented or not applicable (NA); the matched entries are classified by predicted functions (*Right*). (*D*) Venn diagram of overlapping proteins between the lists of Total EV proteins and EV surface proteins (*left*), and correlation assessment between surface proteins in EVs and total protein in EVs (linear model) (*right*). (*E*) Bar graph quantification of fluorescence (MFI) of the cells indicated after incubations with DPP4-Myc EVs and Myc EVs for 24 h. Incubations with no EVs and with only PBS were included as negative controls. Data are the means ±S.E.M. of 3 biological replicates; student's *t*-test was used to assess significance in two-group comparisons, ***, $p \leq 0.001$.

Fig. S6. (*A*) Senescence was monitored by assessing the SA-β-galactosidase activity (blue) in human WI-38 fibroblasts, human HSkM cells, and rat H9c2 cells. Proliferating cells (P) were compared to cells that were rendered senescent by transduction with a lentivirus to express $HRAS^{G12V}$ and trigger oncogene-induced senescence (OIS) and assayed 8 days later (WI-38), or exposure to 10 Gy ionizing radiation (IR) followed by incubation for 10 days (HSkM, H9c2). (*B*) The levels of the senescence marker protein DPP4 and loading control HSP90 in each of the populations in (*A*) were monitored by western blot analysis. (*C*) Western Blot analysis of the levels of DPP4 in lysates from total EVs isolated from WI-38 fibroblasts in which DPP4 was silenced by incubation with specific siRNAs (siDPP4); siCtrl was included in the control siRNA group. Western blot analysis of the EV marker CD81 and staining of the transfer membrane with Ponceau S were used to monitor sample loading.

Fig. S7. (*A*) Numbers of EVs calculated per cell, measured for 48 h after triggering senescence by transducing $HRAS^{G12V}$ in fibroblasts, compared with the control transduction group. (*B*) Quantitative analysis of the DPP4-positive P-EVs and S(OIS)-EVs after labeling EVs with an antibody against DPP4 conjugated with FITC, as assessed by the Flow NanoAnalyzer platform. The percentages of fluorescent DPP4-EVs relative to total EVs detected are indicated. (*C*) Flow cytometric analysis (*left*) and MFI quantification (*right*) of the uptake of S(OIS)-EVs and P-EVs (as well as control incubations with no EVs and with PBS only) by proliferating WI-38, HaCaT, and HMC3 cells. In (A,C), *, $p \leq 0.05$; **, $p \leq 0.01$; ***, $p \leq 0.001$.

Fig. S8. (*A*) The levels of DPP4, the senescence marker protein p53 (TP53), and loading control ACTB (β-Actin) in H9c2 rat myoblasts that were either left untreated (P) or rendered senescent by

exposure to 10 Gy ionizing radiation (IR) followed by incubation for 10 days were monitored by Western blot analysis. (*B*) Quantitative analysis of the levels of DPP4-expressing P-EVs and IR-EVs prepared from H9c2 cells, as assessed using with FITC-labeled anti-DPP4 antibody and the Flow NanoAnalyzer platform. The percentages of fluorescent DPP4-EVs relative to total EVs detected are indicated. (*C*) Flow cytometric analysis of the uptake of S(IR)-EVs and P-EVs isolated from H9c2 (as well as control incubations with no EVs and PBS only) by proliferating rat H9c2 myoblasts and rat NR8383 macrophages. (*D*) Flow cytometric analysis of the uptake of S(IR)-EVs and P-EVs isolated from HSkM cells (as well as control incubations with no EVs and PBS only) by proliferating HSkM myoblasts. In (C,D), *, $p \leq 0.05$; **, $p \leq 0.01$; ***, $p \leq 0.001$.

Fig. S9. Flow cytometric analysis of the uptake of S(RS)-EVs and P-EVs isolated from WI-38 fibroblasts (as well as control incubations with no EVs and with PBS only) by WI-38 fibroblasts 16 h later in the absence or presence of DPP4 inhibitors Diprotin A or Sitagliptin used at the indicated concentrations. These data are reflected in Fig. 5E.

Dataset S1. Total EVs proteomic raw counts
Dataset S2. Total EVs proteomic analysis, particle numbers for normalization
Dataset S3. Total EVs proteomic analysis output
Dataset S4. EVs Surface Proteins raw data Summary
Dataset S5. Surface Protein-PEV-1 raw data
Dataset S6. Surface Protein-PEV-2 raw data
Dataset S7. Surface Protein-PEV-3 raw data
Dataset S8. Surface Protein-RSEV-1 raw data
Dataset S9. Surface Protein-RSEV-2 raw data
Dataset S10. Surface Protein-RSEV-3 raw data
Dataset S11. Surface Protein-IREV-1 raw data
Dataset S12. Surface Protein-IREV-2 raw data
Dataset S13. Surface Protein-ETOEV-1 raw data
Dataset S14. Surface Protein-ETOEV-2 raw data
Dataset S15. EVs surfaceome, proteomic analysis output

Supplementary References

1. G. Midekessa *et al.*, Zeta Potential of Extracellular Vesicles: Toward Understanding the Attributes that Determine Colloidal Stability. *ACS Omega* **5**, 16701-16710 (2020).
2. X. Zhang *et al.*, Proteome-wide identification of ubiquitin interactions using UbIA-MS. *Nat Protoc* **13**, 530-550 (2018).
3. Y. Zhou *et al.*, Metascape provides a biologist-oriented resource for the analysis of systems-level datasets. *Nat Commun* **10**, 1523 (2019).
4. P. Shannon *et al.*, Cytoscape: a software environment for integrated models of biomolecular interaction networks. *Genome Res* **13**, 2498-2504 (2003).
5. Bausch-Fluck D, Goldmann U, Müller S, *et al*., The in silico human surfaceome. *Proc Natl Acad Sci USA*. **115**(46): E10988-E10997 (2018).
6. Almén, Markus Sällman *et al.*, Mapping the human membrane proteome: a majority of the human membrane proteins can be classified according to function and evolutionary origin. *BMC biology* vol. **7**, 50 (2009).

A

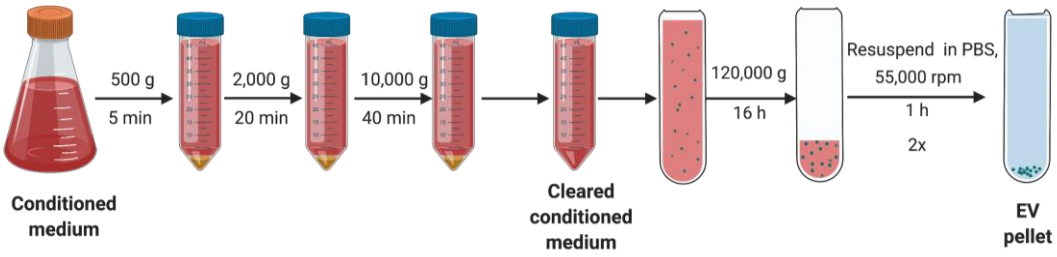
500 g
5 min
2,000 g
20 min
10,000 g
40 min
120,000 g
16 h
Resuspend in PBS,
55,000 rpm
1 h
2x
Conditioned medium
Cleared conditioned medium
EV pellet

B

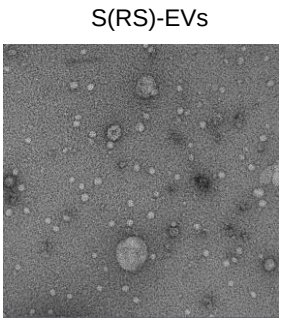
S(RS)-EVs

C

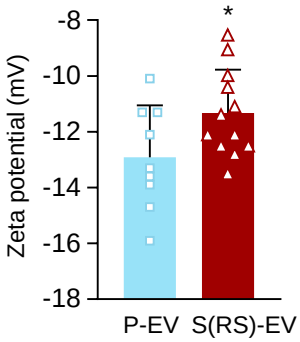
Zeta potential (mV)
-8
-10
-12
-14
-16
-18
*
P-EV
S(RS)-EV

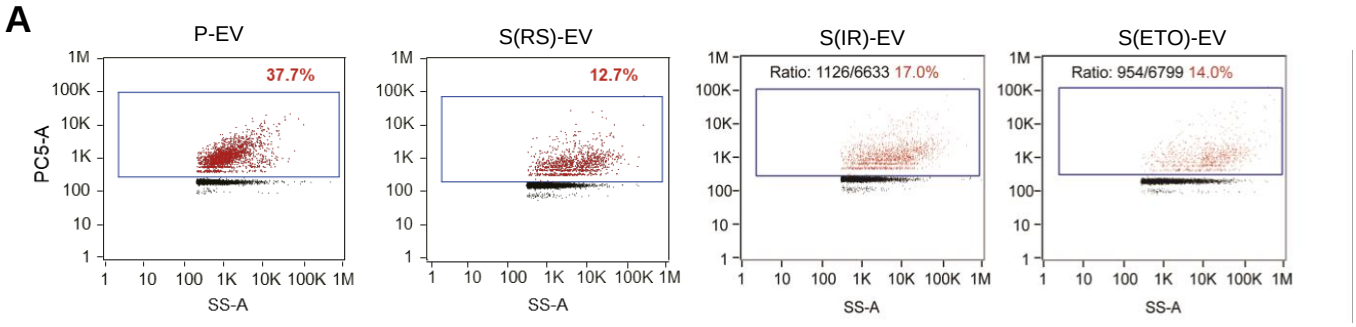
A
P-EV
S(RS)-EV
S(IR)-EV
S(ETO)-EV
37.7%
12.7%
Ratio: 1126/6633 17.0%
Ratio: 954/6799 14.0%
PC5-A
SS-A
1M
100K
10K
1K
100
10
1
1 10 100 1K 10K 100K 1M

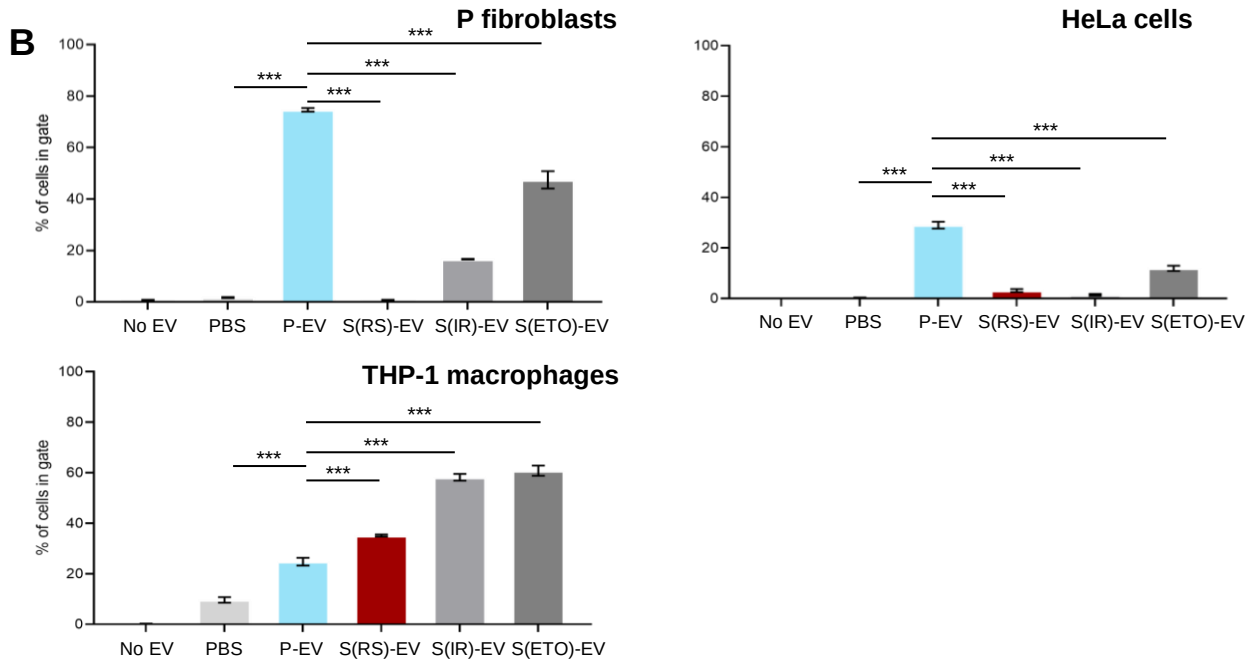
B
P fibroblasts
HeLa cells
THP-1 macrophages
% of cells in gate
***
No EV
PBS
P-EV
S(RS)-EV
S(IR)-EV
S(ETO)-EV

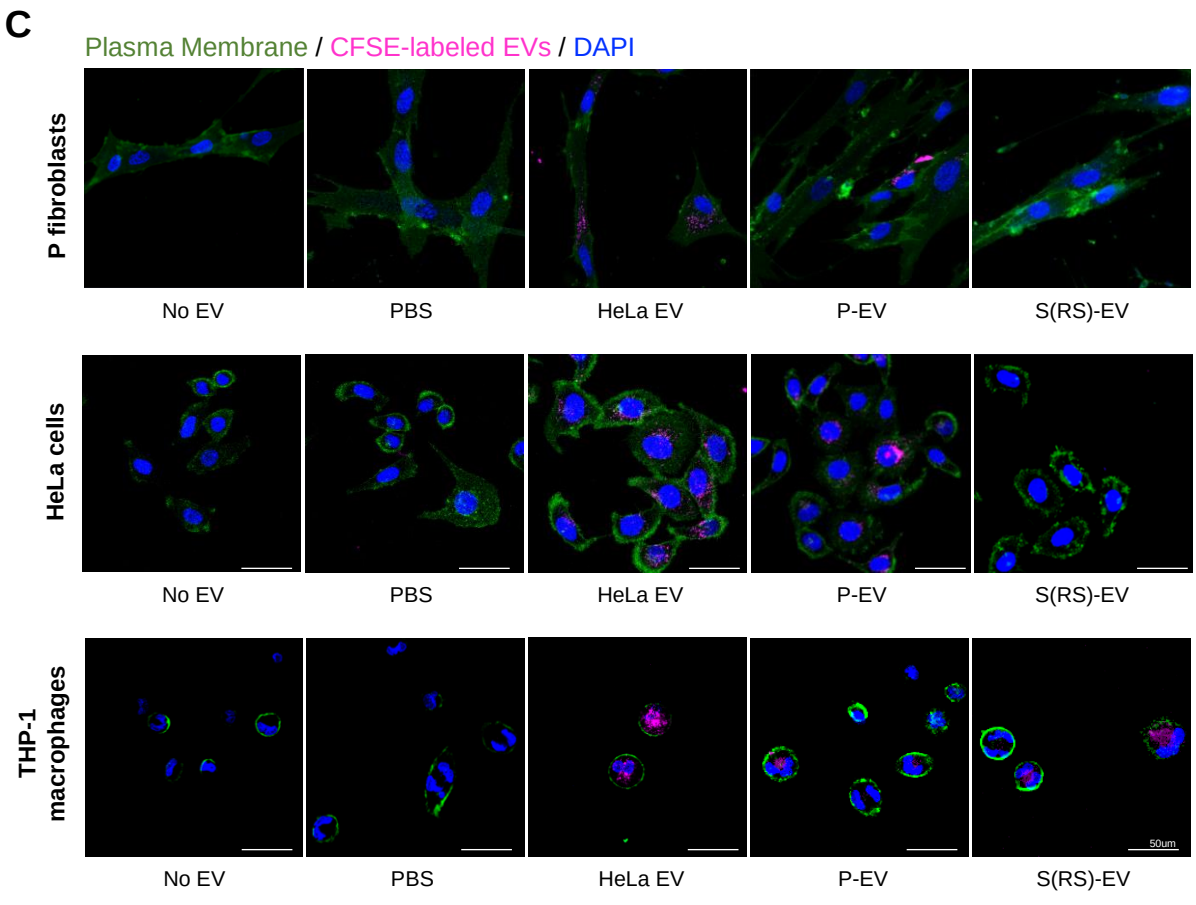
C
Plasma Membrane / CFSE-labeled EVs / DAPI
P fibroblasts
HeLa cells
THP-1 macrophages
No EV
PBS
HeLa EV
P-EV
S(RS)-EV
50um

A

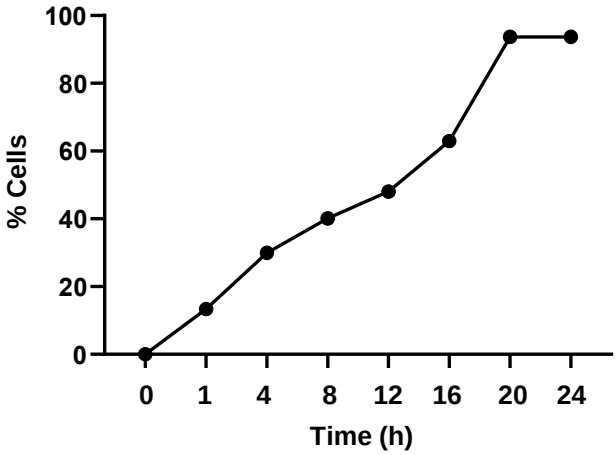
100
80
60
40
20
0
% Cells
0
1
4
8
12
16
20
24
Time (h)

B

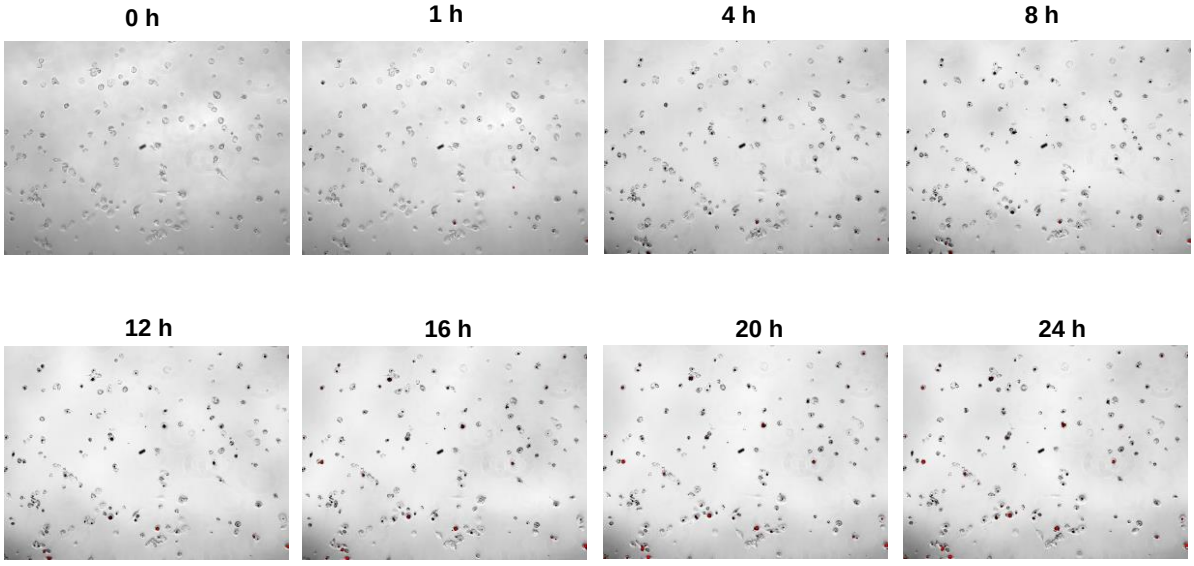
0 h
1 h
4 h
8 h
12 h
16 h
20 h
24 h

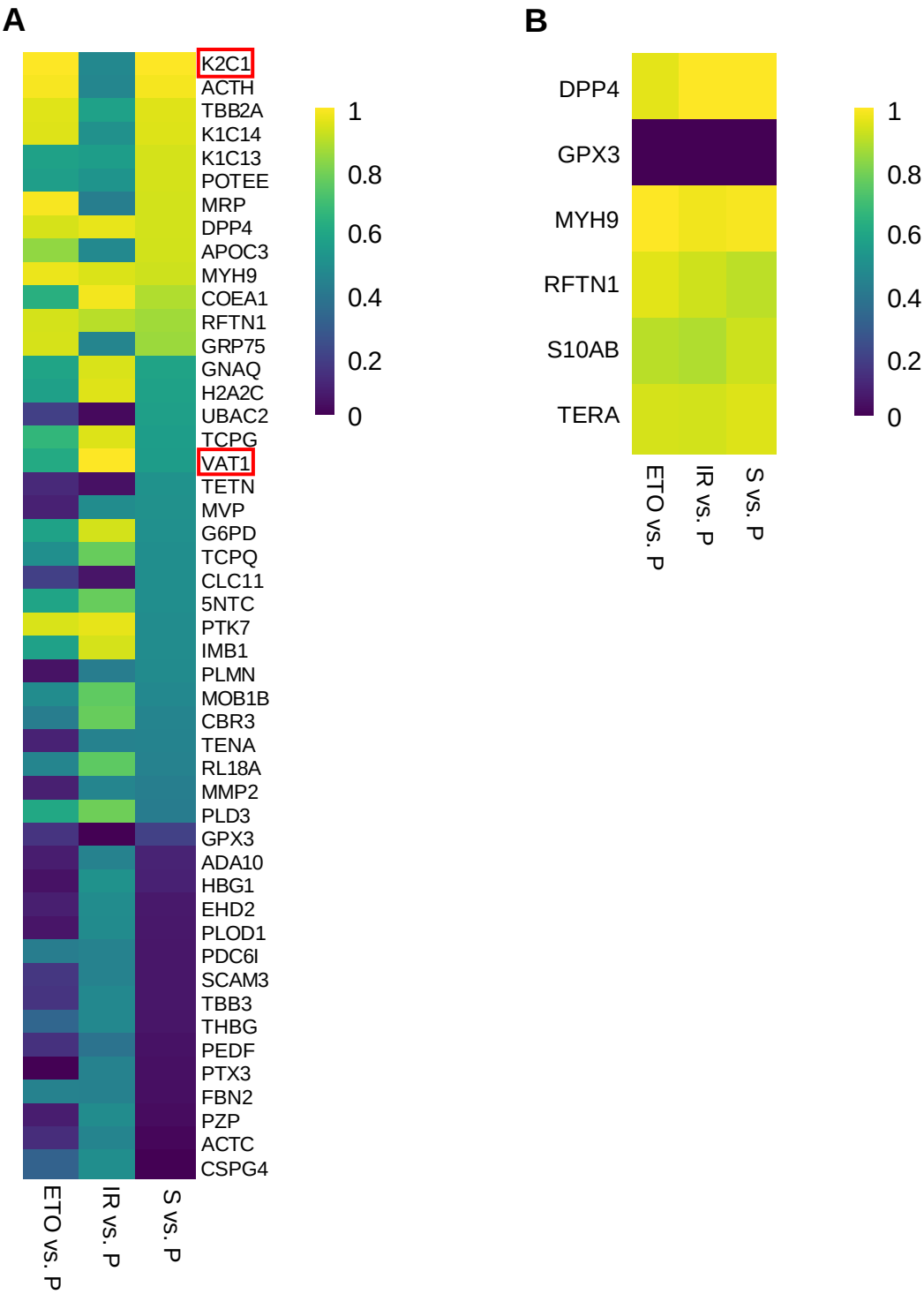
A
K2C1
ACTH
TBB2A
K1C14
K1C13
POTEE
MRP
DPP4
APOC3
MYH9
COEA1
RFTN1
GRP75
GNAQ
H2A2C
UBAC2
TCPG
VAT1
TETN
MVP
G6PD
TCPQ
CLC11
5NTC
PTK7
IMB1
PLMN
MOB1B
CBR3
TENA
RL18A
MMP2
PLD3
GPX3
ADA10
HBG1
EHD2
PLOD1
PDC6I
SCAM3
TBB3
THBG
PEDF
PTX3
FBN2
PZP
ACTC
CSPG4
ETO vs. P
IR vs. P
S vs. P
1
0.8
0.6
0.4
0.2
0
B
DPP4
GPX3
MYH9
RFTN1
S10AB
TERA
ETO vs. P
IR vs. P
S vs. P
1
0.8
0.6
0.4
0.2
0

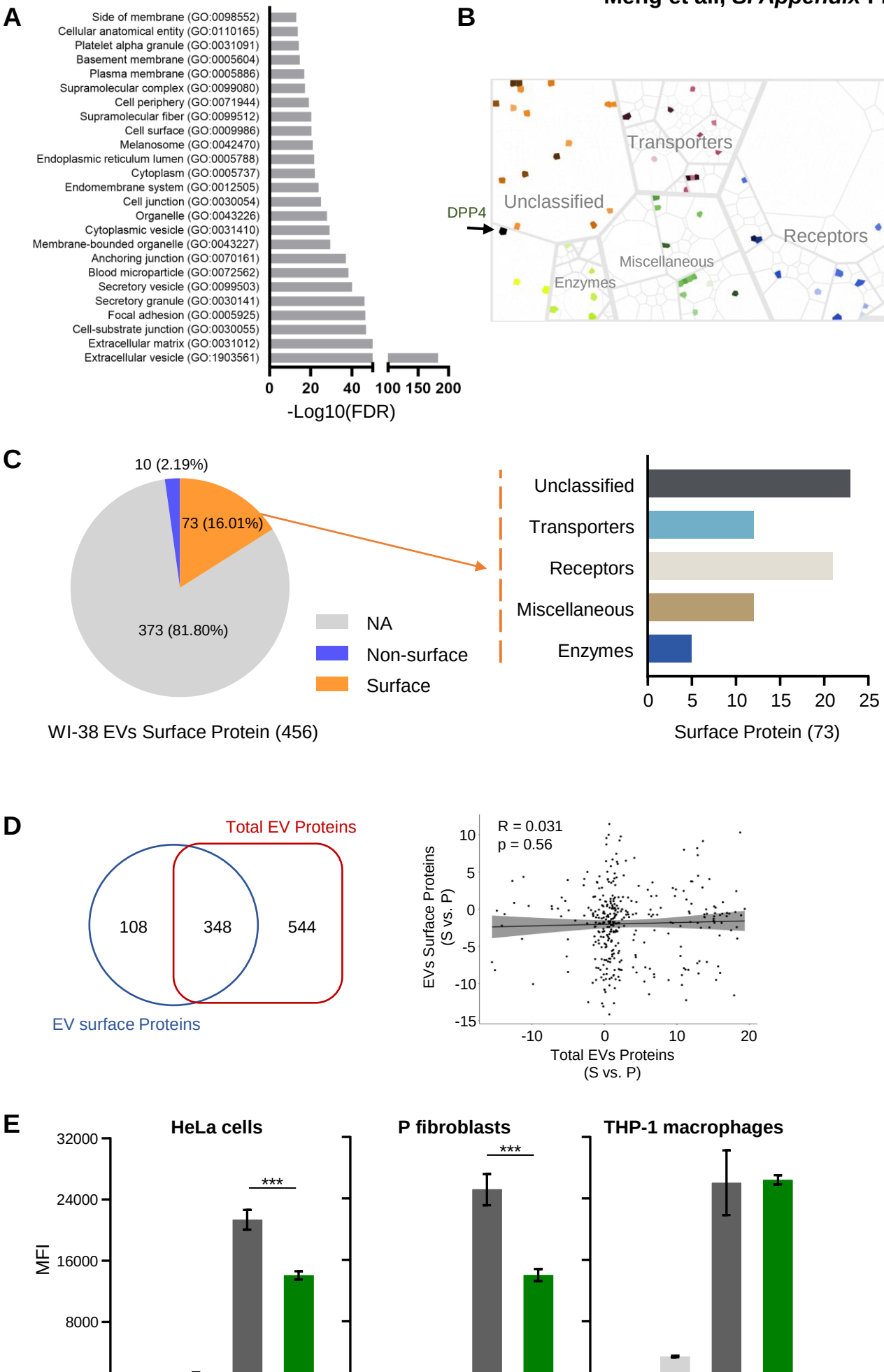
A
Side of membrane (GO:0098552)
Cellular anatomical entity (GO:0110165)
Platelet alpha granule (GO:0031091)
Basement membrane (GO:0005604)
Plasma membrane (GO:0005886)
Supramolecular complex (GO:0099080)
Cell periphery (GO:0071944)
Supramolecular fiber (GO:0099512)
Cell surface (GO:0009986)
Melanosome (GO:0042470)
Endoplasmic reticulum lumen (GO:0005788)
Cytoplasm (GO:0005737)
Endomembrane system (GO:0012505)
Cell junction (GO:0030054)
Organelle (GO:0043226)
Cytoplasmic vesicle (GO:0031410)
Membrane-bounded organelle (GO:0043227)
Anchoring junction (GO:0070161)
Blood microparticle (GO:0072562)
Secretory vesicle (GO:0099503)
Secretory granule (GO:0030141)
Focal adhesion (GO:0005925)
Cell-substrate junction (GO:0030055)
Extracellular matrix (GO:0031012)
Extracellular vesicle (GO:1903561)
0 20 40 100 150 200
-Log10(FDR)
B
Transporters
Unclassified
DPP4
Receptors
Miscellaneous
Enzymes
C
10 (2.19%)
73 (16.01%)
373 (81.80%)
NA
Non-surface
Surface
WI-38 EVs Surface Protein (456)
Unclassified
Transporters
Receptors
Miscellaneous
Enzymes
0 5 10 15 20 25
Surface Protein (73)
D
Total EV Proteins
108
348
544
EV surface Proteins
R = 0.031
p = 0.56
EVs Surface Proteins (S vs. P)
10 5 0 -5 -10 -15
-10 0 10 20
Total EVs Proteins (S vs. P)
E
HeLa cells
P fibroblasts
THP-1 macrophages
MFI
32000 24000 16000 8000 0
***
***
No EV
PBS
Myc EV
DPP4 EV

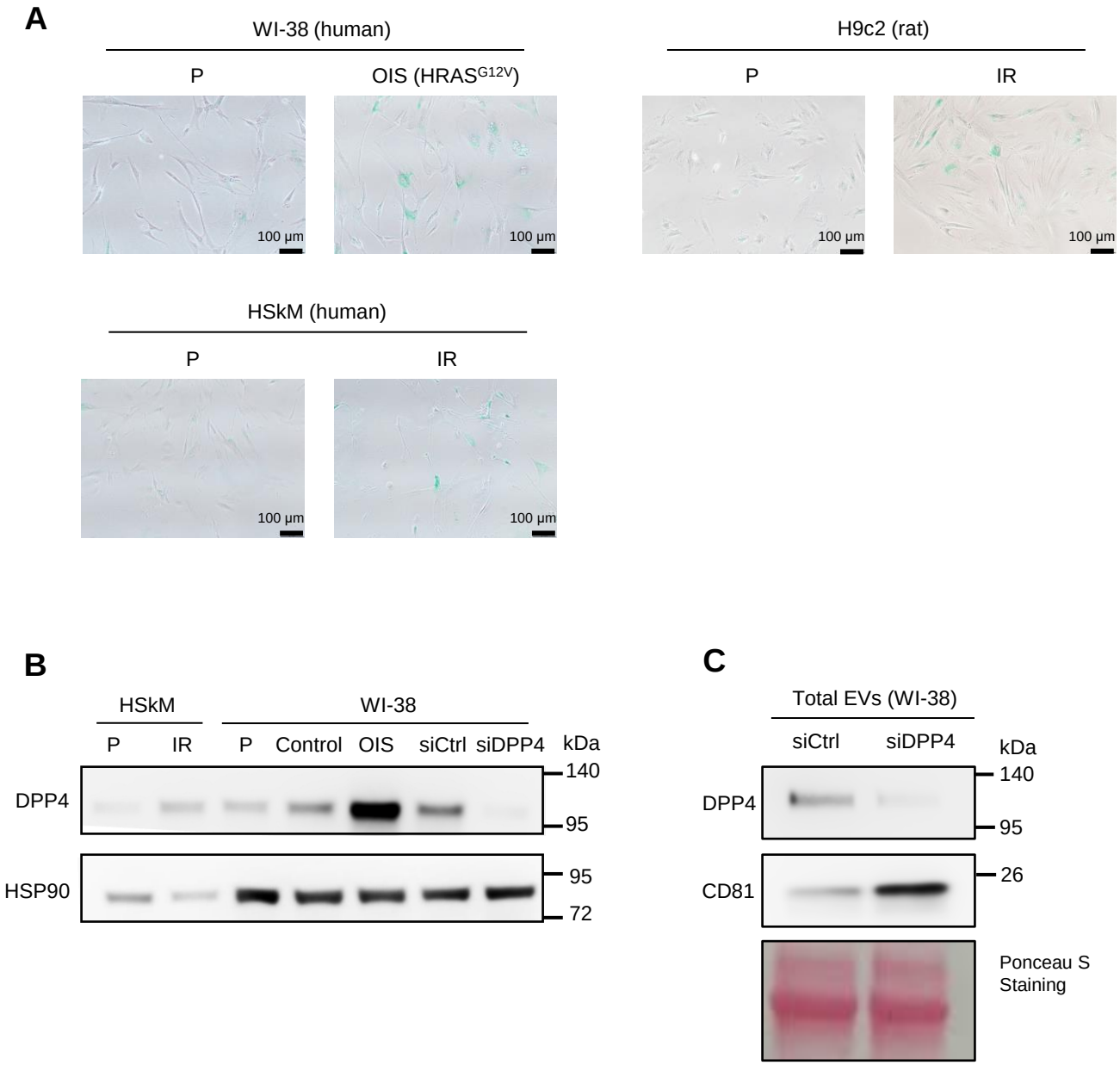
A
WI-38 (human)
P
OIS (HRAS^{G12V})
H9c2 (rat)
P
IR
HSkM (human)
P
IR
100 μm
B
HSkM
WI-38
P
IR
P
Control
OIS
siCtrl
siDPP4
kDa
DPP4
140
95
HSP90
95
72
C
Total EVs (WI-38)
siCtrl
siDPP4
kDa
DPP4
140
95
CD81
26
Ponceau S
Staining

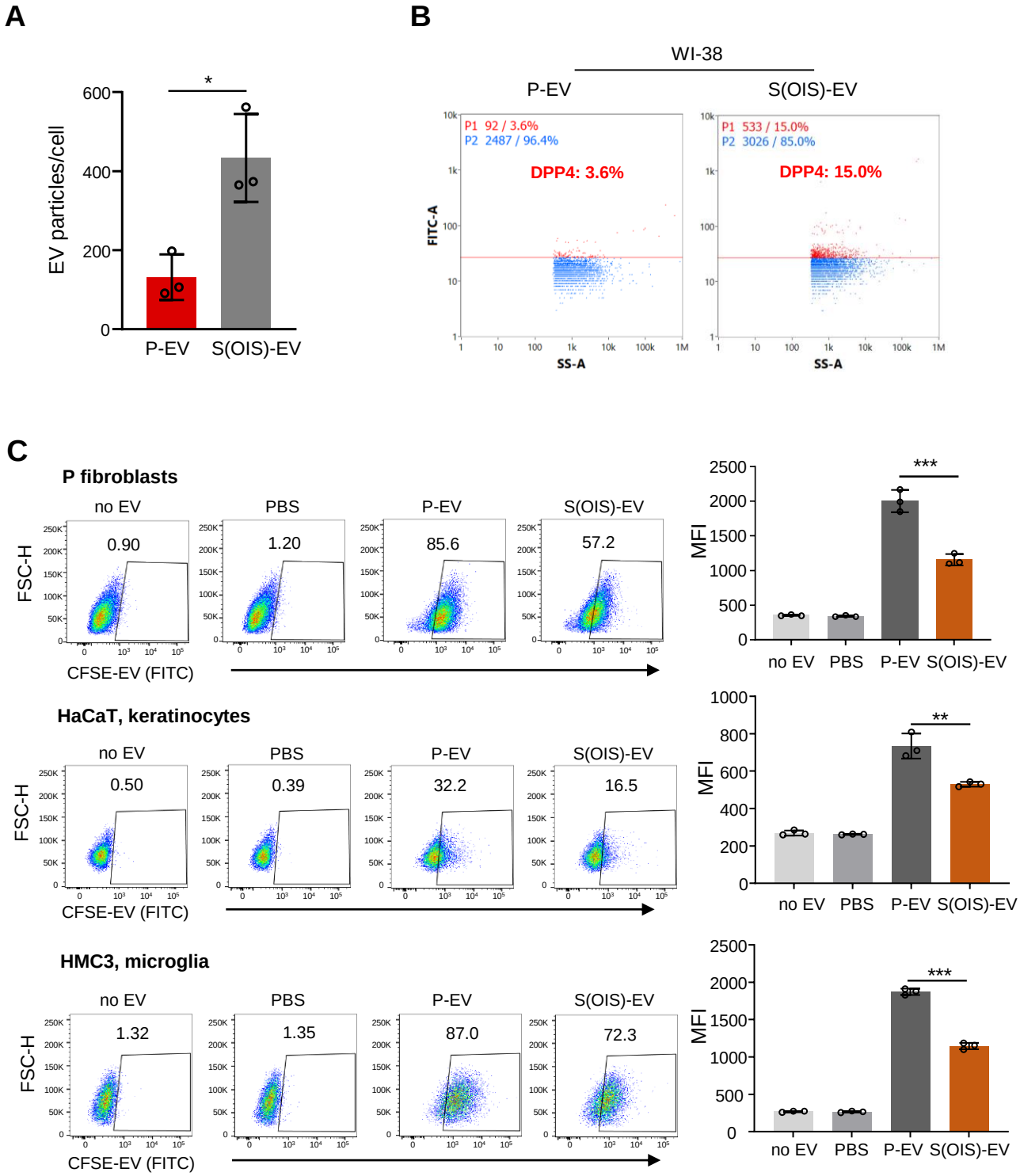
A
EV particles/cell
600
400
200
0
*
P-EV
S(OIS)-EV
B
WI-38
P-EV
S(OIS)-EV
P1 92 / 3.6%
P2 2487 / 96.4%
DPP4: 3.6%
P1 533 / 15.0%
P2 3026 / 85.0%
DPP4: 15.0%
FITC-A
SS-A
C
P fibroblasts
no EV
PBS
P-EV
S(OIS)-EV
0.90
1.20
85.6
57.2
FSC-H
CFSE-EV (FITC)
MFI
***
HaCaT, keratinocytes
0.50
0.39
32.2
16.5
**
HMC3, microglia
1.32
1.35
87.0
72.3
***

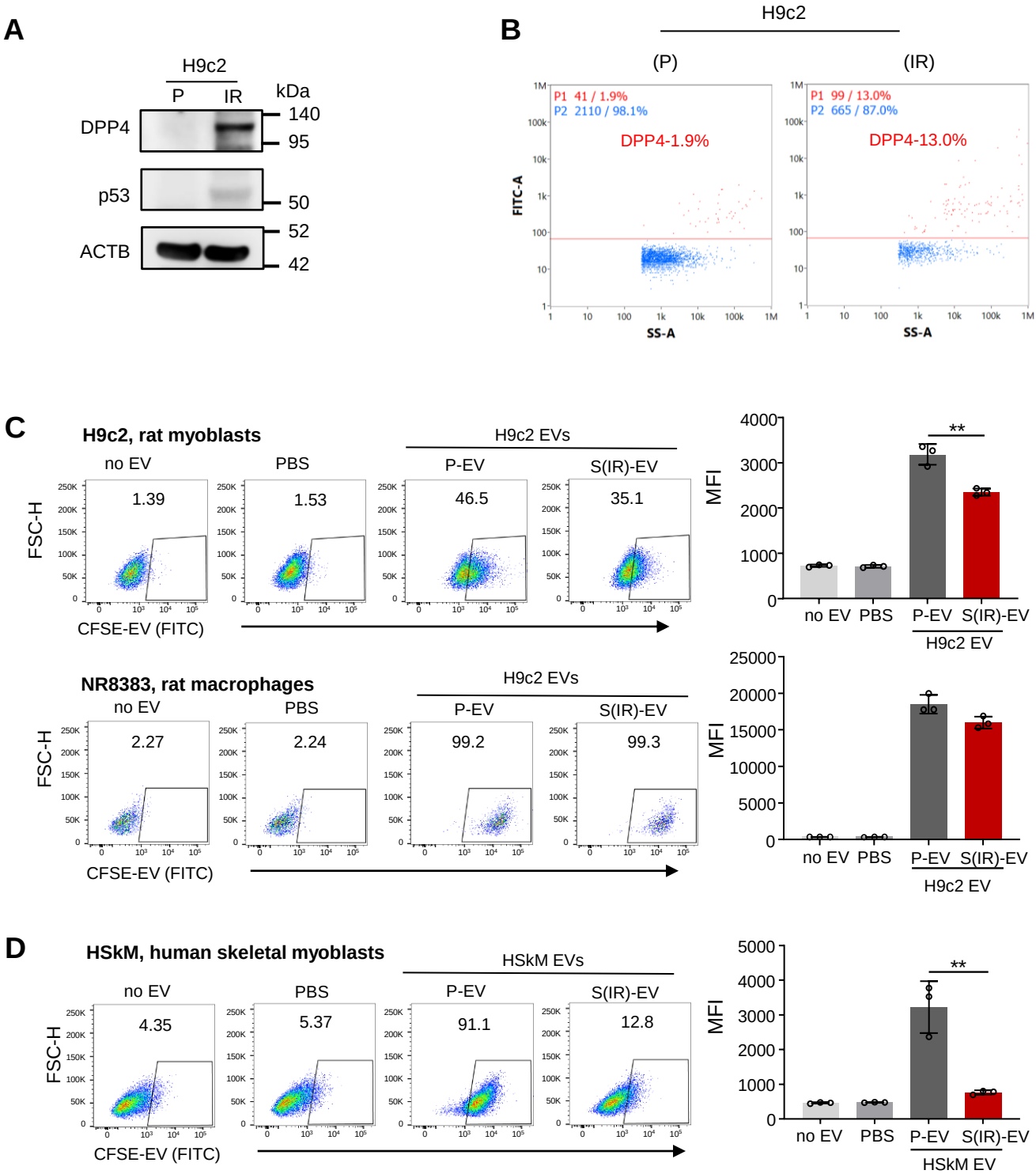
A
H9c2
P
IR
kDa
DPP4
140
95
p53
50
ACTB
52
42
B
H9c2
(P)
(IR)
P1 41 / 1.9%
P2 2110 / 98.1%
DPP4-1.9%
P1 99 / 13.0%
P2 665 / 87.0%
DPP4-13.0%
FITC-A
SS-A
C
H9c2, rat myoblasts
H9c2 EVs
no EV
PBS
P-EV
S(IR)-EV
1.39
1.53
46.5
35.1
FSC-H
CFSE-EV (FITC)
MFI
**
no EV
PBS
P-EV
S(IR)-EV
H9c2 EV
NR8383, rat macrophages
2.27
2.24
99.2
99.3
D
HSkM, human skeletal myoblasts
HSkM EVs
4.35
5.37
91.1
12.8
HSkM EV

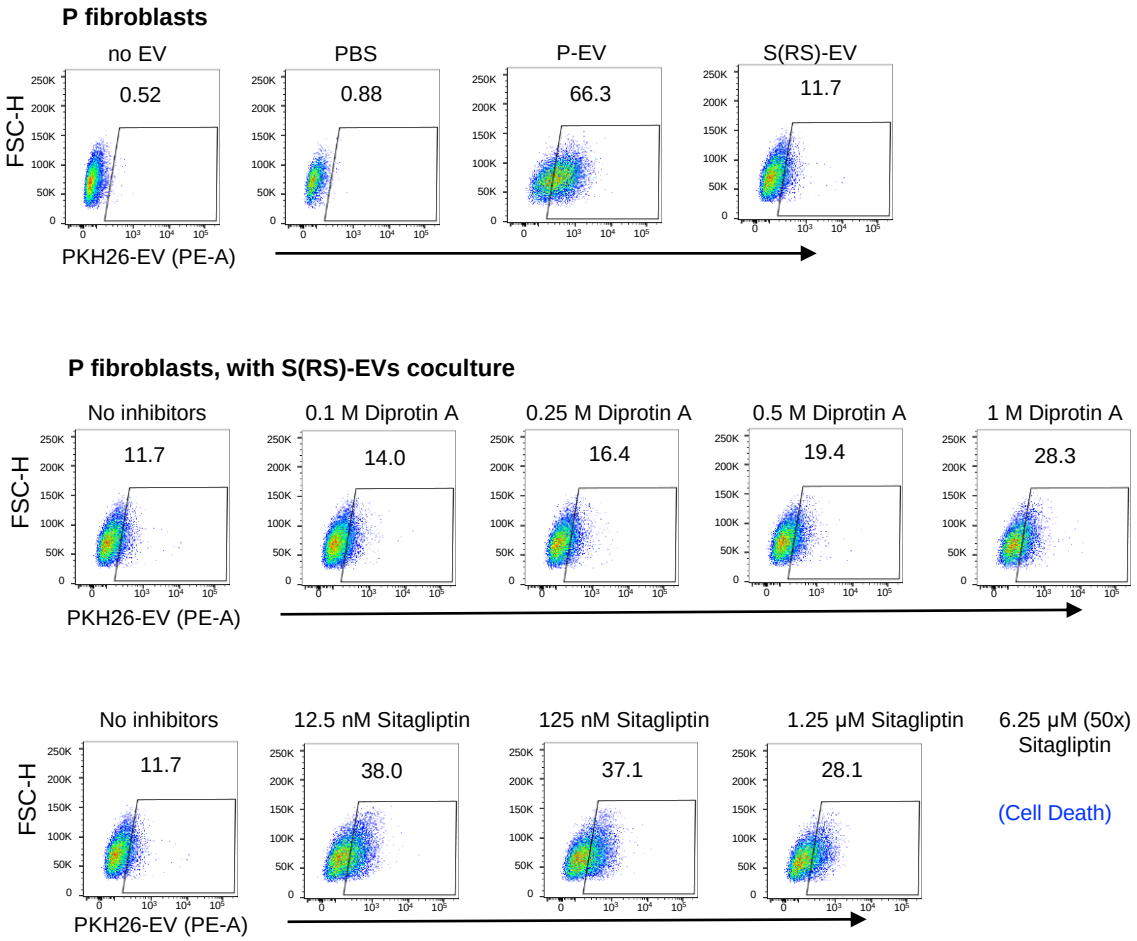
P fibroblasts
no EV
PBS
P-EV
S(RS)-EV
0.52
0.88
66.3
11.7
FSC-H
PKH26-EV (PE-A)
P fibroblasts, with S(RS)-EVs coculture
No inhibitors
0.1 M Diprotin A
0.25 M Diprotin A
0.5 M Diprotin A
1 M Diprotin A
11.7
14.0
16.4
19.4
28.3
FSC-H
PKH26-EV (PE-A)
No inhibitors
12.5 nM Sitagliptin
125 nM Sitagliptin
1.25 μM Sitagliptin
6.25 μM (50x) Sitagliptin
11.7
38.0
37.1
28.1
(Cell Death)
FSC-H
PKH26-EV (PE-A)